energies

MDPI

Article

Aerogel Product Applications for High-Temperature Thermal Insulation

Alexander V. Fedyukhin [1,*], Konstantin V. Strogonov [1], Olga V. Soloveva [2], Sergei A. Solovev [3], Irina G. Akhmetova [3], Umberto Berardi [4], Mark D. Zaitsev [1] and Daniil V. Grigorev [1]

[1] Energy Efficiency and Hydrogen Technology Department, Moscow Power Engineering Institute, National Research University, 111250 Moscow, Russia
[2] Institute of Heat Power Engineering, Kazan State Power Engineering University, 420066 Kazan, Russia
[3] Institute of Digital Technologies and Economics, Kazan State Power Engineering University, 420066 Kazan, Russia
[4] Department of Architectural Science, Toronto Metropolitan University, Toronto, ON M5B 2K3, Canada
* Correspondence: fediukhinav@mpei.ru

Abstract: This paper presents the results of theoretical and experimental studies to determine the optimal thickness of thermal insulation from basalt fiber and aerogel products for pipelines at temperatures of 300 and 600 °C. We carried out a comparison of the key thermophysical characteristics of the claimed heat-insulating materials. We performed a thermal imaging survey of the furnace chimney, insulated with basalt fiber and aerogel, while controlling the temperature of the flue gases by establishing the required ratio of the flow rate of natural gas and oxidizer. The temperature gradient along the thickness of the thermal insulation was obtained using a numerical tool developed in ANSYS. The results show that aerogel surpasses basalt fiber in all key thermophysical characteristics. At the same time, the only barrier to widespread industrial production and use of aerogel in the high-temperature thermal insulation segment is its market cost, which is still several times higher than that of basalt fiber in terms of an equivalent performance.

Keywords: high-temperature thermal insulation; aerogel; basalt fiber; thermal conductivity; natural gas furnace

Citation: Fedyukhin, A.V.; Strogonov, K.V.; Soloveva, O.V.; Solovev, S.A.; Akhmetova, I.G.; Berardi, U.; Zaitsev, M.D.; Grigorev, D.V. Aerogel Product Applications for High-Temperature Thermal Insulation. *Energies* **2022**, *15*, 7792. https://doi.org/10.3390/en15207792

Academic Editors: Alan K. T. Lau, Artur Blaszczuk, Baohua Jia and Chan Yi Jing

Received: 12 September 2022
Accepted: 17 October 2022
Published: 21 October 2022

1. Introduction

The use of aerogel in the world is very extensive as aerogel is used in construction, medicine, transportation, metallurgical and aerospace fields, acoustics, electrical and military industries. The widespread use of aerogel is due to its unique set of properties: high porosity, low density, low thermal conductivity and dielectric constant [1]. Aerogels based on carbon fiber, silica aerogels, cellulose aerogels and graphene aerogels are among the most common ones [2]. Despite the numerous methods for synthesizing aerogels of various compositions, researchers continue to improve the structure and properties, as well as reduce the cost for the production of existing aerogels and develop new types of aerogels. The essence of all studies on increasing the efficiency of using aerogel as a heat-insulating material is to reduce the thermal conductivity, improve its resistance to mechanical stress and increase the uniformity of the structure.

Yang et al. studied various insulating materials reinforced with aerogel [3]. In the course of the work, they analyzed the morphology of the studied samples, the influence of humidity and ambient temperature on thermal conductivity. It was found that the aerogel content is inversely proportional to the thermal conductivity of the composite material. The thermal conductivity of the samples is less affected by changes in ambient temperature at low and medium humidity but increases significantly with a small change in temperature under conditions of extreme humidity. Issues related to the hydrophobicity of the composite material at different aerogel content were also considered.

In the article [4], an effective compromise between the pore size and density of the synthesized pectin aerogels was studied to achieve the lowest thermal conductivity. Groult et al. studied morphology of aerogels by varying the concentrations of calcium and pectin. Researchers gave the features of calcium induction of aerogels to reach a sufficiently large number of macropores. The minimum value of thermal conductivity for the synthesized samples was 0.0147 ± 0.0002 W/m·K.

Aerogel used as an effective thermal insulation must also meet the standards of heat resistance, resistance to mechanical stress, and hydrophobicity. In [5], silica aerogels from monodispersed silica sol were developed and studied. The identified advantages of the developed material include a strong frame structure that prevents the aerogel pores from collapsing, an increase in thermal stability while maintaining low thermal conductivity. Thus, aerogel samples retain their structure at temperatures up to 900 °C and have a relatively small degree of shrinkage at 1000 °C. In addition, the authors found a reduction in the specific surface area of silica aerogels compared to conventional aerogels.

Cai et al. developed an aerogel based on glucomannan konjac/starch [6]. This study turned out that an increase in the concentration of starch leads to a thickening of the walls of the cells. This improves the thermal insulation properties due to the formation of closed pores. The addition of starch improves the mechanical strength of the aerogel. It was determined that due to limitations in the value of the density of aerogels, the most appropriate concentration of starch is 2%. Thus, the inclusion of wheat straw in the composition of the aerogel makes it possible to control its pore size. In addition, it is proposed to add gelatin as a binding agent to prevent the straw from settling.

Guided by the need for high thermal insulation performance and mechanical resistance of thermal insulation materials, researchers [7] developed cross-linked polyimide aerogels with SiO_2 nanoparticles. The specific compression modulus of the developed material was 334 kN·m·kg^{-1}. Cross-linking agents make it possible to achieve uniform porosity and stability of the aerogel structure. The material demonstrates good thermal insulation properties in a wide temperature range from 20 °C to 300 °C.

Nguyen et al. were engaged in the processing of rice straw into aerogel [8]. PVA and cationic starch (PVA and cationic starch) were used as binder products. Taking into account the fact that the initial raw material was used for production, the finished aerogel samples are highly porous (0.97%), light, have good hydrophobicity and low thermal conductivity (0.034 W/m·K). These characteristics are maintained even after prolonged exposure to the environment. The method of making aerogel samples consisted of freeze-drying to give the aerogel a particular shape.

Meanwhile new research was aimed at the development of aerogel in order to increase its mechanical stability and reduce thermal conductivity [9]. As a result, a wood-based nanofibrillated cellulose aerogel was produced, which showed high porosity (99.4%) and low density (8.1 kg/m^3). Gupta et al. recorded change in thermal conductivity when changing the concentration of cellulose. The method described in the article for the synthesis and modification of aerogels from nanofibrillated cellulose is simple and cheap compared to other known methods of synthesis. In turn, a negative feature of this method is an increase in the thermal conductivity of the synthesized product.

The development of aerogel from zirconium oxide stabilized with yttrium oxide was carried out in the article [10]. Yoon et al. considered the manufactured product (YSZ) as a thermal insulator for the surface of a gas turbine. Thermal conductivity of aerogel at 1000 °C was 0.212 W/m·K. The resistance of the material to high-temperature exposure was confirmed in the preservation of the nanoporous structure. The average pore size of the material samples was about 11 nm.

Despite the fact that foam concrete is increasingly used in the construction of buildings, it is necessary to reduce its thermal conductivity and density in order to be able to use it more widely. Li et al. were engaged in the production and description of ultralight aerogel foam concrete [11]. Various additives were added to the composition of the material, such as a foaming agent, a thickener, etc. The density and thermal conductivity values of the

fabricated material are 198 kg/m^3 and 0.049 W/(m·K), respectively. Li et al. concluded that by changing the content of cement and aerogel powder, it is possible to effectively reduce the thermal conductivity of the material.

Iswar et al. studied the need for aerogel aging to reduce its shrinkage, the possibility of producing an aerogel with low thermal conductivity and ensuring the reducibility of the material [12]. The study was carried out by X-ray microtomography.

Wei et al. considered the factors affecting the effective thermal conductivity of the aerogel and composite material based on the aerogel, the possibility of radiative heat transfer through the material with nanopores [13]. Wei et al. found the value of aerogel density at which the thermal conductivity coefficient is minimal.

Lakatos et al. considered the persistence of the physical properties of the aerogel depending on the humidity and ambient temperature [14]. The period of optimal use of insulation and the change in physical properties over this period were investigated. Berardi et al. also considered the impact of aging and environmental conditions on the effective thermal conductivity of thermal insulation [15]. Lakatos et al. considered the methods of using aerogel, which belongs to the group of advanced porous materials, as thermal insulation of enclosing structures [16]. Lakatos et al. solved the problems of condensate precipitation in case of heterogeneity of the resistance of the enclosing structure, associated with the effect of a thermal bridge. Tugnoli et al. developed a physical model for calculating the effective thermal conductivity under conditions as close as possible to the operating conditions of a high-temperature aerogel in a wide range of temperatures and void fractions [17].

Yang et al. carried out a numerical and experimental study of the thermal characteristics of aerogel insulating panels to improve the energy efficiency of buildings [18]. The numerical study revealed the dependence of the influence of pores on the thermal characteristics of the material. The correctness of the model was confirmed by comparison with the obtained experimental data.

Fesmire et al. developed a multilayer composite insulation system for non-vacuum applications and extreme environmental conditions [19]. The aerogel coating system can be used for both space launches and cryogenic engine test facilities, and is to provide suitable thermal insulation for complex cryogenic pipelines.

Wei et al. studied the thermal conductivity of granular and powdered silica aerogels at various temperatures and pressures [20]. The dependence of the influence of macropores on the change in thermal conductivity with increasing pressure and temperature was revealed.

Liao et al. considered a method for using graphene aerogel as a matrix for encapsulating a material with a phase transition (PCM) [21]. The use of graphene aerogel gives the composite structure the ability to retain its original shape and prevent PCM leaks above the melting point. Kazemi et al. studied the effect of PCM on the thermal insulation characteristics of the aerogel [22].

Liu et al. developed an optimization framework based on a genetic algorithm for designing the geometric structure of silica aerogel composites, which used microscale opacifiers and fibers to block infrared radiation with a wavelength of 3 to 8 μm [23]. The authors declare the possibility of using a composite material as a high-temperature thermal insulation.

Zhang et al. proposed a new method for obtaining graphene aerogel; by reducing the electrical conductivity of the material, it can be used as electrical insulation [24].

Hu et al. obtained an yttrium-alumina aerogel using inorganic precursors [25]. The thermal insulation characteristics, microstructure, and morphology of yttrium-alumina aerogel were studied [26].

Typical materials for the formation of inorganic aerogels are oxides of metals such as silicon, aluminum, titanium, zirconium, hafnium, yttrium, vanadium, etc. Aerogel is mainly used in combination with other materials, which improves its basic properties, for example, to reduce transmission of infrared radiation, potassium titanate six can be used [27]. Methods for joining the components of a composite material using aerogel can

be conditionally divided into two options: introduction before drying under supercritical conditions, either at the stage of gel formation, or into a gel filled with an appropriate solvent, and introduction of reinforcing components after drying under supercritical conditions into the finished aerogel, which is most often obtained using the technology of supercritical media.

In the field of energy saving buildings, aerogel is used in glazing similar to conventional double glazing, where the air cavity between two transparent glass panels is filled with silicon dioxide aerogel. In addition, aerogel enhanced thermal insulation mats are used in buildings to minimize thermal bridges. The use of mats with a thickness of 10 to 20 mm leads to a reduction in energy consumption by about 22 and 16% for concrete and steel buildings, respectively [28]. In addition to the construction industry, aerogel-enhanced insulation is used in industry, in particular in steel ladles. As the thermal insulation material of the ladle, a material consisting of nanosized silicon powder with a thermal conductivity of 0.031 W/m·K at 800 °C was used, which is 0.042 W/m·K lower than that of traditional insulation (basalt fiber). As a result, the ladle temperature drop rate decreased by 0.12–0.13 °C/min, which ultimately led to a reduction in the cost of producing a ton of steel by about 60 rubles [29].

To assess the long-term characteristics of materials using aerogel, laboratory studies were carried out on the accelerated aging of materials. The materials have been subjected to the following critical environmental stresses to achieve results similar to 20 years of standard operating conditions: solar radiation, i.e., ultraviolet (UV), visible (VIS) and near infrared (NIR) radiation; ambient infrared (IR) thermal radiation; extreme temperatures; temperature changes/cycles; water, e.g., humidity, relative humidity, rain (precipitation); physical activity, imitation of snow and wind; pollution, dirt, and dust; microorganisms, mold, and bird droppings. As a result of the experiments, heat-insulating gypsum showed the greatest increase in thermal conductivity. At a high level of humidity (70% vol.), the thermal conductivity of aerogel-reinforced gypsum increased by 10% and reached a value of 0.035 W/m·K, a thermal conductivity comparable to that of insulating materials such as polyisocyanurate and expanded polystyrene. Among all aerogel-reinforced products evaluated, mats and fiberboards demonstrated superior performance in both unaged and long-term conditions [30]. Amorphous SiO_2 aerogel embedded in a glass mesh after annealing to 250 °C increased its thermal conductivity to 0.02 W/m K (from 0.017 W/m·K), and when annealed at 70 °C for 6 weeks showed no changes [31]. When exposed to combustion products at adiabatic flame temperatures above 2000 K, the material degrades according to three main mechanisms: loss of glass fiber content, sintering of the silica aerogel structure, and partial melting of the aerogel structure [32].

Carbon aerogel, which has an ultra-low thermal conductivity of only about 0.12 W/m·K at a temperature of about 2000 K, at a temperature of 2700 K gives a maximum effective total thermal conductivity of about 0.16 W/m·K, which is five to ten times lower than generally accepted high-temperature thermal insulation materials, such as carbon, fibrous felt or carbon foam, currently available [33].

2. Relevance of the Research

Technological needs of the industry consume half of all thermal energy produced in the Russian Federation, mainly in the form of steam. The largest consumers of thermal energy are enterprises of the chemical, petrochemical, fuel, metallurgical, machine-building, processing and food industries. Many large industrial enterprises in the energy-intensive industries listed above have a complex and extensive energy supply system. The main share of thermal energy consumption is accounted for by water vapor used for technological needs of production. For such enterprises, measures aimed at reducing heat losses during the transportation of energy carriers are promising. The temperature range in which industrial insulation structures operate is from −180 to 600 °C. Industrial thermal insulation is used for thermal insulation of systems transporting high-temperature coolants, the vast

majority (85–90%) of which is assembled from fibrous materials (basalt fiber and fiberglass products) [34].

In the segment of low-temperature thermal insulation (up to 150 °C), polyurethane foam is the dominant thermal insulation material in heat networks [35,36]. While in construction and high temperature zones (300–600 °C) for thermal insulation of steam networks and technological equipment, basalt fiber mats are the main-used material due to ease of installation and low cost [37–39]. At the same time, basalt fiber has the following disadvantages that aerogel lacks: a significant increase in the thermal conductivity with increasing temperature, a limitation on the maximum application temperature (usually up to 600 °C), mechanical deformations and damage during long-term operation. Nominally, aerogel surpasses basalt fiber in all key thermophysical and operational characteristics. Therefore, the only barrier to widespread industrial production and use of aerogel in the high-temperature thermal insulation segment is its market value, which, as a rule, is several times higher than the price of basalt fiber in terms of an equivalent volume of material.

Currently, the cost of thermal insulation based on aerogel is on average 1.5–2.5 times higher than the cost of basalt fiber (comparing the capital costs of insulation materials for one linear meter of pipeline under the same temperature conditions). At the same time, the nominal service life of thermal insulation based on aerogel is usually 3 times higher than basalt fiber. In this case, the operating cost of thermal insulation based on aerogel in 25–30 years becomes lower than basalt fiber, which requires replacement every 7–10 years.

3. Materials and Methods

3.1. Experimental Study

In this work, the following samples were investigated: basalt fiber of the URSA brand and aerogel of the Aspen Aerogels brand. According to the declared technical characteristics, both materials can be used as high-temperature thermal insulation for industrial technological installations. Experimental studies were carried out with the application of samples on a chimney with a diameter of 150 mm of the furnace (Figure 1), in which natural gas was burned.

(**a**) (**b**)

Figure 1. Natural gas furnace: (**a**) General view; (**b**) Chimney.

Operational regulation of natural gas and airflow allowed us to establish two stationary regimes of the experiment: with flue gas temperatures at the base of the chimney of 300 and 600 °C. Figure 2 shows a thermal image of an uninsulated chimney at a stationary temperature regime of 300 °C. Figures 3 and 4 show examples of thermal imaging pictures of thermal insulation surfaces at stationary temperature conditions of 300 and 600 °C, respectively.

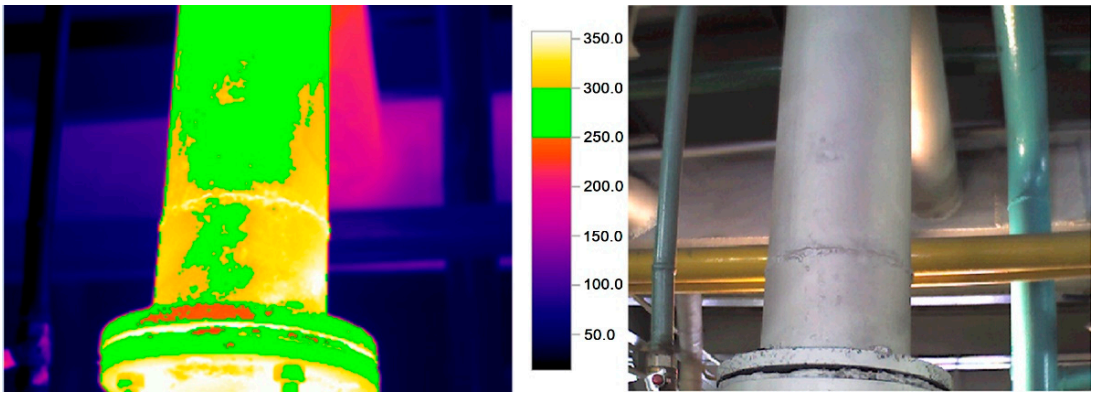

Figure 2. Thermal imaging of the chimney at 300 °C.

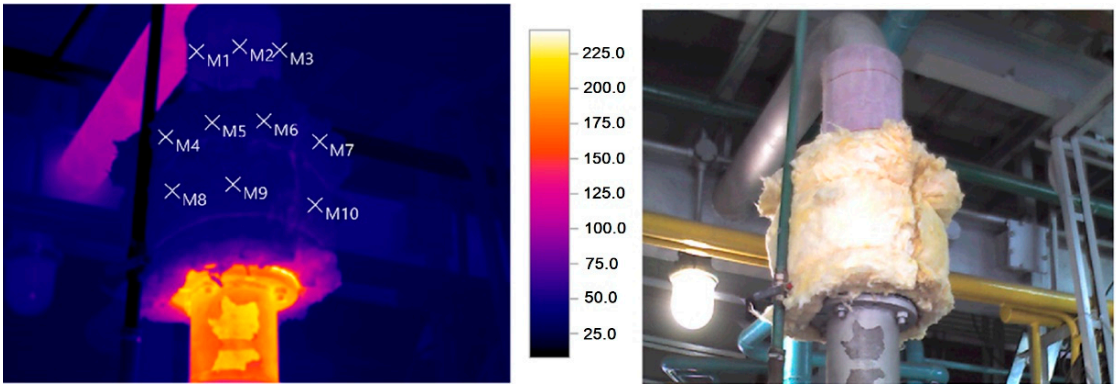

Figure 3. Thermal imaging of an insulated chimney at 300 °C: measurements values (°C) are M1—48.1; M2—46.1; M3—43.9; M4—35.0; M5—34.7; M6—36.2; M7—40.5; M8—37.3; M9—42.0; M10—46.0.

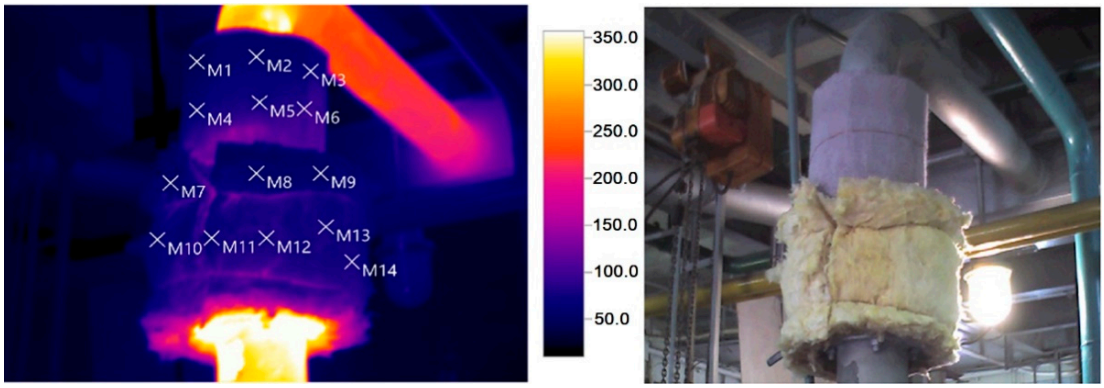

Figure 4. Thermal imaging of an insulated chimney at 600 °C, measurements (°C): M1—47.5; M2—59.6; M3—72.0; M4—63.9; M5—76.2; M6—81.2; M7—54.0; M8—58.1; M9—56.8; M10—61.1; M11—70.9; M12—79.0; M13—74.8; M14—80.2.

A series of temperature measurements on the surface of insulating materials was carried out. Temperature values can vary greatly at different points on the surface. This may

be due to uneven heating of the pipe surface and convective airflows near the insulation. We presented the results of measurements in Table 1.

Table 1. The results of measurements.

Pipe Surface Temperature, °C	Insulation Surface Temperature, °C			Average Deviation
	T Min	T Max	T Average	
		Aerogel		
300	43.9	51.4	47.3	1.6
600	44.6	81.2	62.9	9.1
		Basalt fiber		
300	34.7	53.2	41.2	4.5
600	53.6	80.2	64.7	8.4

Table 1 shows that the average temperature on the surface of the aerogel is greater than the average temperature on the surface of the basalt fiber for the case of a pipe temperature of 300 °C. In this case, the average temperature on the surface of the aerogel is less than the average temperature on the surface of the basalt fiber for the case of a pipe temperature of 600 °C. This may be due to the incorrect choice of the thickness of the insulating material used.

The thicknesses of thermal insulation for the corresponding regimes were used equal: 20 and 60 mm for aerogel (operating manual for Aspen Aerogel Pyrogel XT material), 150 and 225 mm for basalt fiber (SP 41-103-2000). Figure 5a shows graphs of insulating material thickness versus temperature for a 150 mm diameter pipe according to selected documents; Figure 5b demonstrates the thermal conductivity of a material as a function of temperature.

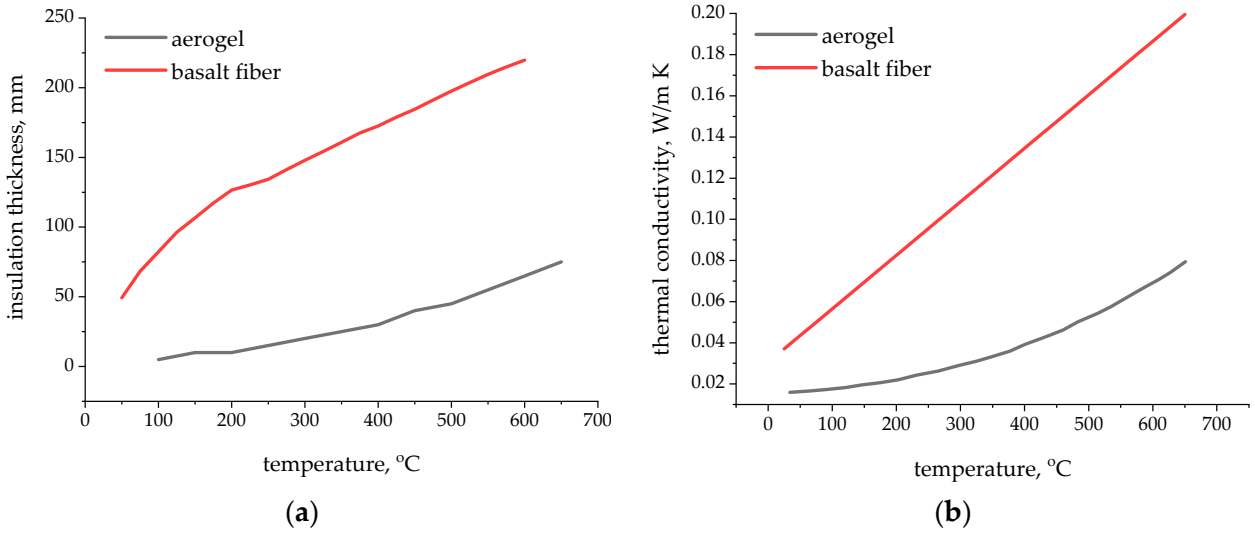

Figure 5. Parameters of insulating materials according to technical documentation: (**a**) minimum thickness; (**b**) thermal conductivity.

Figure 5 shows that at high temperatures, the recommended minimum insulation thickness varies almost linearly. In addition, the linear law of change has a dependence of the thermal conductivity of basalt fiber on temperature. In this case, the change in the thermal conductivity for aerogel at high temperatures is essentially non-linear.

Following the previous results, additional studies of the thermal conductivity of existing aerogel samples using laboratory measuring equipment in the temperature range of 40–90 °C were carried out. Figure 6 shows the layout of the laboratory setup and the measurement results. Differences from passport data do not exceed 6%.

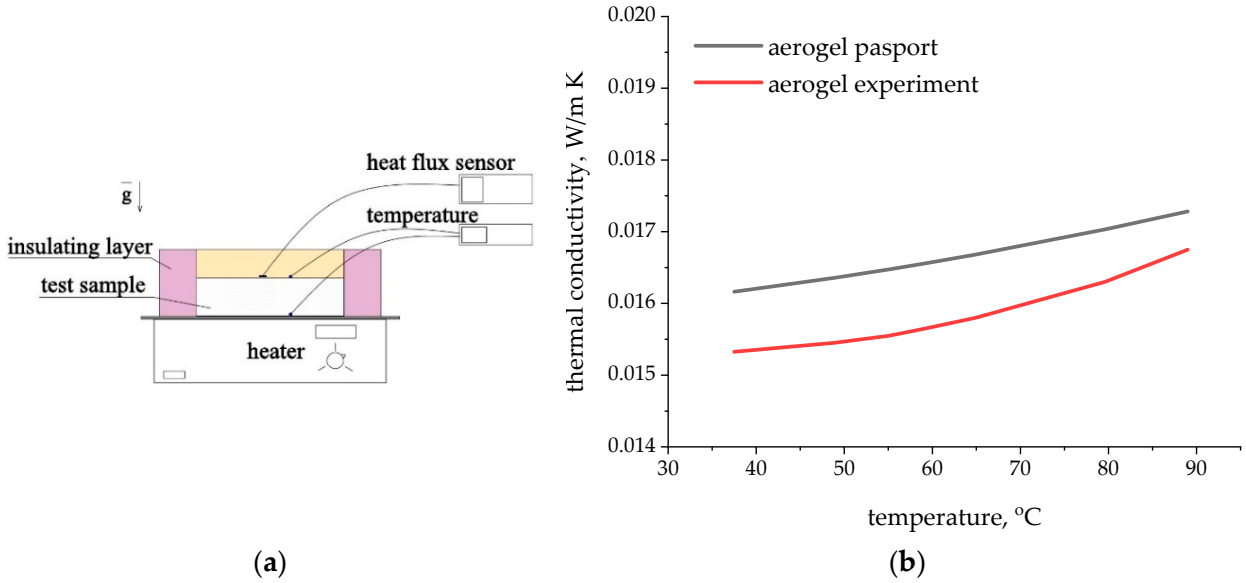

Figure 6. Laboratory measurements of aerogel thermal conductivity: (**a**) experimental setup; (**b**) thermal conductivity.

A thermal imaging method was used to experimentally determine the surface temperature of an insulated and non–insulated chimney (Figures 2–4) [40]. The results obtained made it possible to verify the standard values of thermal insulation thicknesses for the corresponding materials. At the same time, such methods as fault detection algorithm for pipeline insulation layer based on immune neural network [41], pipeline image diagnosis algorithm based on neural immune ensemble learning [42], pipeline image segmentation algorithm and heat loss calculation based on gene-regulated apoptosis mechanism [43] are innovative methods contactless diagnostics of the pipelines are redundant for solving the tasks set out in this article. Therefore, we preferred the standard thermal imaging method for determining exclusively the surface temperature of pipelines.

3.2. Numerical Simulation

For additional analysis of experimental data and properties of insulating materials, numerical simulation was carried out in the ANSYS software package. As a basic equation, consider the transfer of thermal energy through an insulating solid material. As a mechanism for heat transfer in a solid, we have thermal conductivity. We write the energy conservation equation as

$$\nabla(k\nabla T(x,y,z)) = 0,$$

where T is temperature in the insulating material at a point (x,y,z), k is thermal conductivity coefficient of insulating material. The thermal conductivity parameters of the insulating material correspond to the values from Figure 5b.

For simulation, we choose a simplified model of the section of the insulating pipe. Let us consider the transfer of heat from the pipe to the environment in the approximation of an infinite cylindrical wall. Figure 7a shows the computational domain. To simplify, we will select one quarter of the pipe section, which will further speed up the calculations. On the border of the quarter cut, we set the symmetry condition. Consider heat transfer only through insulating material. From the side of the heated pipe, we set the condition of constant temperature $T_p = \text{const}$.

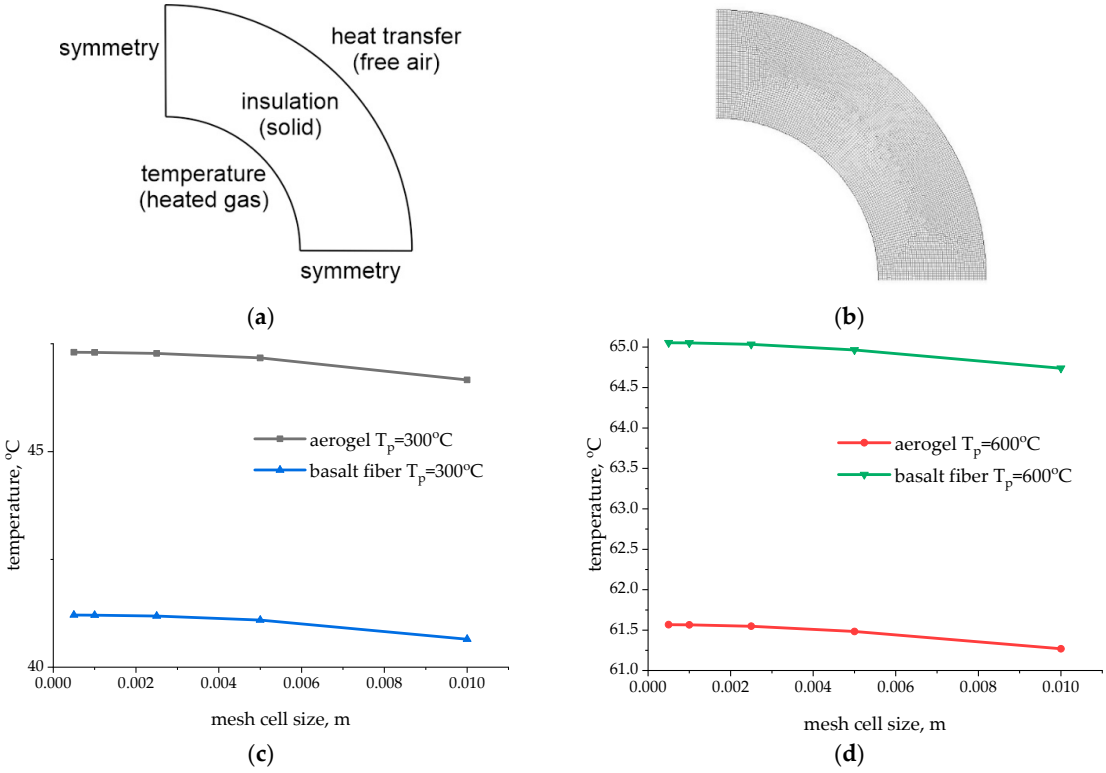

Figure 7. Parameters of numerical simulation: (**a**) Computational domain; (**b**) Mesh example; (**c**) Dependence of the temperature on the insulation surface on the size of the mesh element for the temperature of the pipe 300 °C; (**d**) Dependence of the temperature on the insulation surface on the size of the mesh element for the temperature of the pipe 600 °C.

ANSYS software was used for simulation and Fluent module used for finite volume method. The parameters are not changed over time as the model is chosen to be stationary. We used the following algorithm to conduct a large series of numerical simulations:

- Creation of a geometric model of the computational domain in the shape of one quarter of the pipe section. We only change the thickness of the insulation.
- Meshing. The choice of the optimal mesh size is presented later in this section.
- Setting the parameters of the insulating material in accordance with the requirements of the software. In the present study, we varied the value of the thermal conductivity coefficient.
- Specifying boundary conditions. We varied the temperature on the side of the heated pipe.
- Calculation. We used the standard Simple algorithm. We considered that the calculation converged when the residual for the energy conservation equation became less than 10^{-12}.
- Determination of the calculated temperature value on the outer surface of the insulating material.

Due to the geometric shape of the pipe and the formulation of the problem, it is sufficient to use 1D analysis, where heat transfer occurs in the radial direction. We use the ANSYS, which provides the verified models and methods. Since the software used only works with 2D or 3D geometric models, we chose a quarter circle in the 2D model approximation. The choice of a quarter circle allows you to provide real boundary conditions.

From the side of the ambient air, we set the condition for convective heat transfer. The operating furnace and open sections of pipes provide additional heating of the air around the insulating material in the installation under study. Using the experimental data, we selected the values of the ambient air temperature and the heat transfer coefficients

of the aerogel and basalt fiber. For a heated gas temperature in the pipe of 300 °C, the ambient air temperature is 32.7 °C. For a heated gas temperature in a pipe of 600 °C, the ambient air temperature is 48.2 °C. Additional intermediate ambient temperature values are obtained by linear approximation. The obtained heat transfer coefficients for aerogel are 16.35 W/m^{2}K, for basalt fiber heat transfer coefficient is 9.2 W/m^{2}K.

Since a very simple geometric model and a simple stationary heat transfer model were chosen in this study, we limited ourselves to choosing the optimal mesh size.

The computational domain was covered with a quadrangular grid. An analysis of the grid partition was carried out to select the optimal cell size. Figure 7c,d shows the results of calculating the temperature at the surface of the insulating material for cases corresponding to experimental studies for aerogel and basalt fiber. One can see differences in temperature values for different cell sizes. The differences in the results for the considered variants of cell sizes are small and do not exceed 2%, but when the cell size is less than 0.001 m, the differences in the results become less than 0.01%. Therefore, meshing with a cell size of 0.001 m was chosen for calculations. ANSYS Fluent (v. 19.2) software was used to solve the model described above.

4. Results and Discussion

Figure 8 shows the results of modeling heat transfer through the thermal insulation layer for 300 and 600 °C, respectively. Obviously, the use of aerogel leads to an insignificant increase in the outer diameter of the chimney, while basalt fiber increases the outer diameter by more than twice. This factor has a direct effect on the radiating surface: that is, at an equal temperature of the outer wall (usually 50–60 °C), the surface area of the pipeline insulated with basalt fiber will be larger in proportion to the outer diameter, which increases the heat loss from the surface of the high-temperature pipeline or process equipment in the enterprise. This aspect is extremely important for reducing heat losses in the steam networks of large oil refineries.

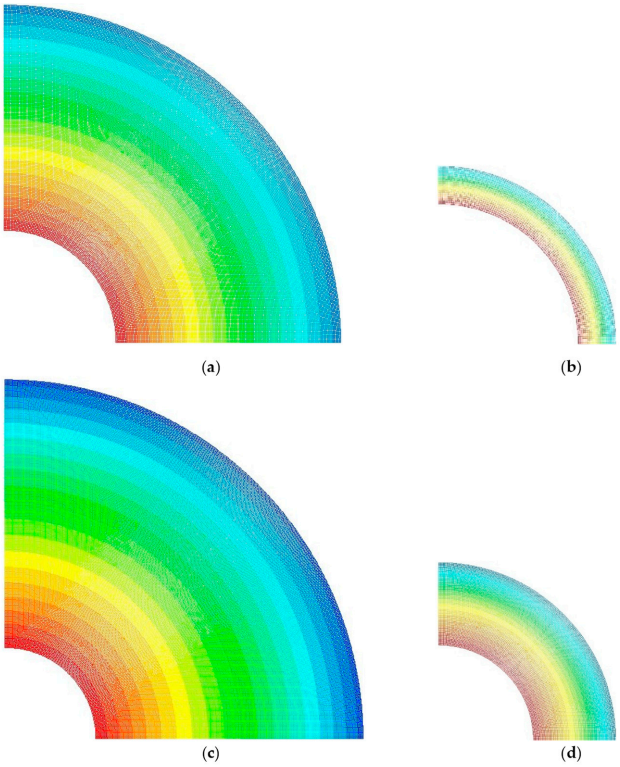

Figure 8. Temperature field based on simulation results for pipe temperature 300 and 600 °C: (**a**) Basalt fiber, T_p = 300 °C; (**b**) Aerogel, T_p = 300 °C; (**c**) Basalt fiber, T_p = 600 °C; (**d**) Aerogel, T_p = 600 °C.

Further, we made calculations for the use of the investigated insulating materials for the pipe temperature range from 150 to 600 °C. We also consider a wide range of insulating material thicknesses, from 5 mm to 80 mm for aerogel and from 25 mm to 250 mm for basalt fiber. Figure 9 shows the obtained results of the temperature on the surface of the insulating material, depending on the thickness of the insulation. The curves are presented for different temperatures of the heated pipe.

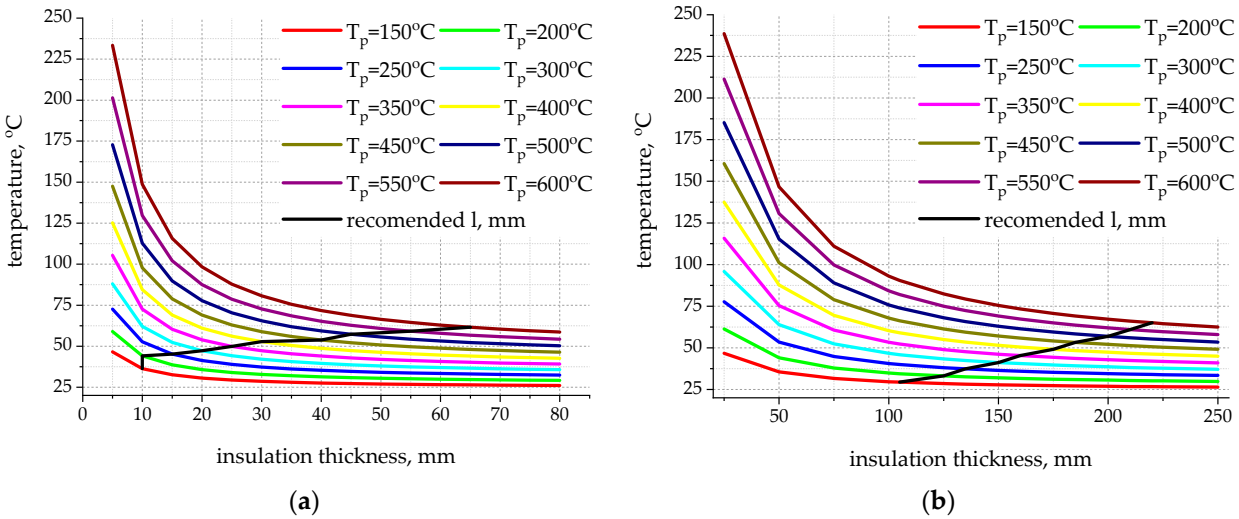

Figure 9. The temperature on the surface of the insulating material depending on the thickness of the insulation and the temperature of the heated pipe for the experimental conditions: (**a**) Aerogel; (**b**) Basalt fiber.

Figure 9 shows that for both aerogel and basalt fiber, using the recommended thickness of the insulating material, we acquire an increase in temperature at the surface of the insulation with increasing temperature of the heated pipe. For aerogel, the temperature on the surface of the insulating material varies from 36.37 °C for T_p = 150 °C to 61.57 °C for T_p = 600 °C. For basalt fiber, the temperature on the surface of the insulating material varies from 29.4 °C for T_p = 150 °C to 65.05 °C for T_p = 600 °C. This is primarily due to the approximation that with an increase in the temperature of the pipe in the experiment, the ambient air temperature increases. Obviously, the passport data and recommendations for choosing the minimum insulation thickness are drawn up for conditions of a fixed ambient temperature, which should not depend on the temperature of the heating device.

The analysis continued carrying out similar calculations, provided that the ambient temperature T_f was constant, with T_f = 20 °C and T_f = 30 °C. The calculation results are shown in Figure 10.

Figure 10 shows that for aerogel at a constant ambient temperature, the temperature on the surface of the insulating material changes slightly: from 31.87 °C to 37.29 °C for T_f = 20 °C, from 41.02 °C to 46.44 °C for T_f = 30 °C. Thus, the use of aerogel insulating material according to passport recommendations makes it possible to provide a temperature on the insulation surface of about 35 °C for T_f = 20 °C and about 45 °C for T_f = 30 °C. For basalt fiber at a constant ambient temperature, the temperature on the surface of the insulating material varies: from 24.6 °C to 37.16 °C for T_f = 20 °C, from 34.34 °C to 47.05 °C for T_f = 30 °C. Thus, the chosen methodology for determining the minimum thickness of basalt fiber does not provide the same temperature values at the surface of the material for the selected sample.

Taking into account the obtained results, we will adjust the choice of the minimum thickness of the insulating material for the samples used in the experimental study. Figure 11 shows the results of choosing the minimum thickness of the insulating material for aerogel and basalt fiber. The graph shows the values from the passport for the studied aerogel, the

values from the manual for basalt fiber (SP 41-103-2000), as well as the results of adjusting the values taking into account the results obtained.

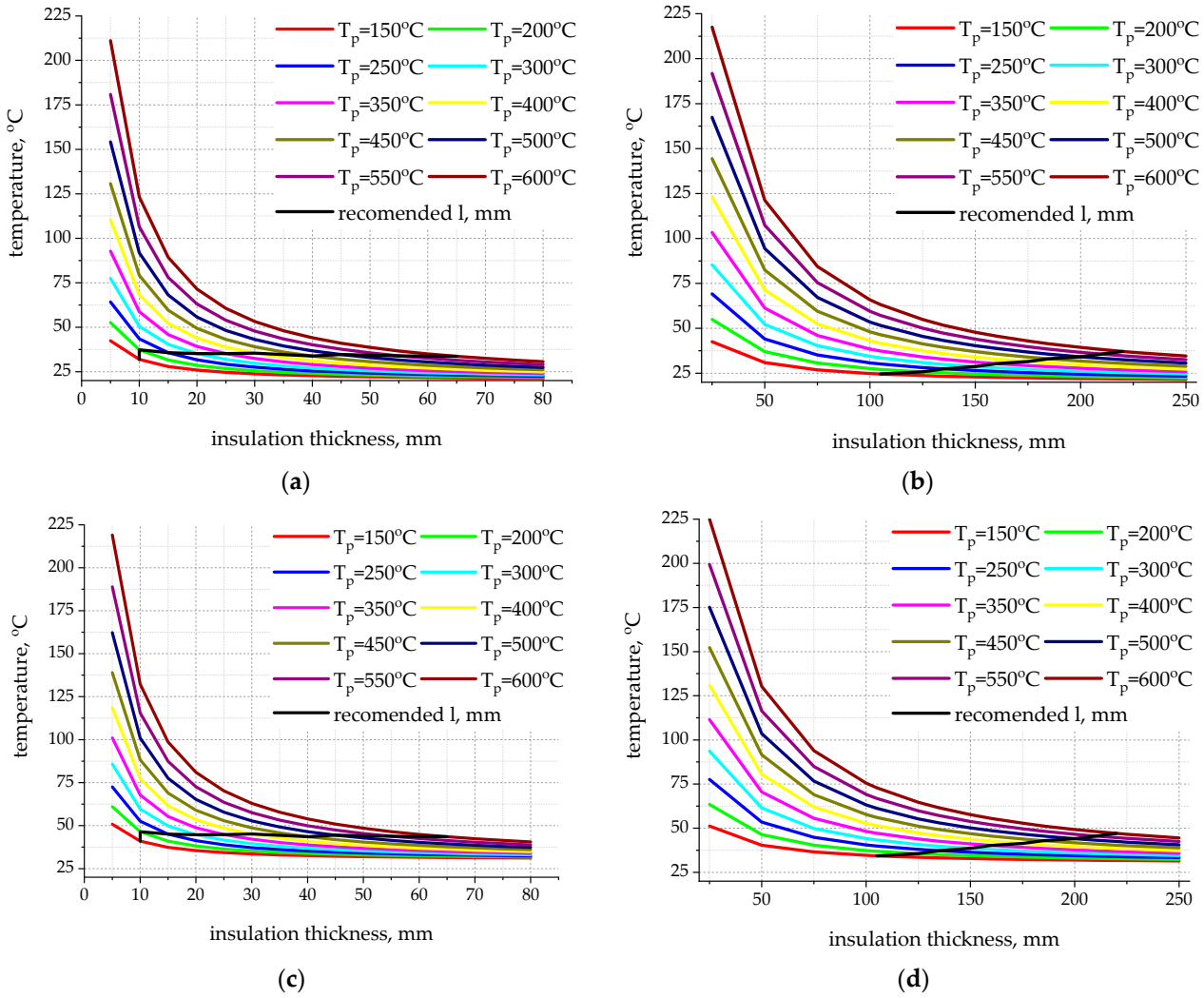

Figure 10. The temperature on the surface of the insulating material depending on the thickness of the insulation and the temperature of the heated pipe for cases T_f = 20 °C and T_f = 30 °C: (**a**) Aerogel, T_f = 20 °C; (**b**) Basalt fiber, T_f = 20 °C; (**c**) Aerogel, T_f = 30 °C; (**d**) Basalt fiber, T_f = 30 °C.

From Figure 11, it can be seen that the calculations show satisfactory values of the aerogel surface temperature when choosing the minimum thickness. At the same time, we can note a slight decrease in the thickness of the insulation in the temperature range of 450–600 °C. For basalt fiber, the adjustment of the minimum insulation thickness is more significant. The choice of modern basalt insulation makes it possible to significantly reduce the thickness of the insulating material at a pipe temperature of up to 500 °C compared to the SP 41-103-2000 methodology. At the same time, for a pipe temperature of 600 °C, the calculated minimum insulation thickness is significantly greater than the recommendations of the chosen methodology. Note that the resulting graph of the minimum insulation thickness has a similar behavior with the behavior of the thermal conductivity value from Figure 5b.

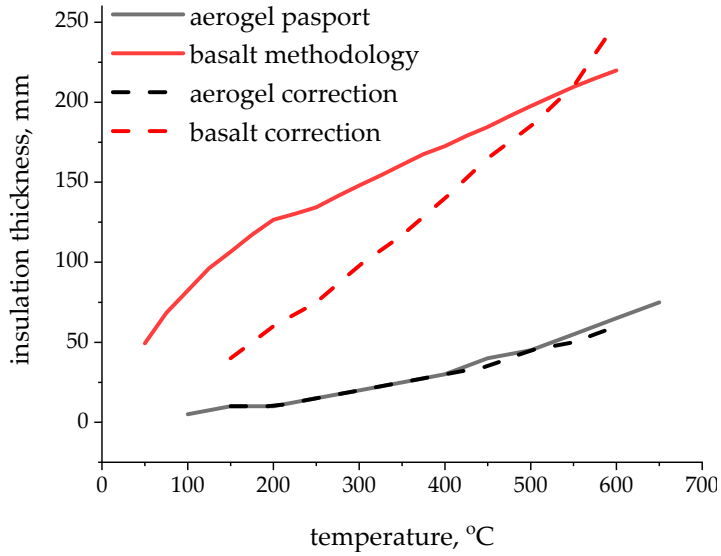

Figure 11. The minimum thickness of the studied insulating materials, taking into account the adjustment from numerical simulation.

Thus, if the data on the recommended insulation thickness are unknown or the passport data are doubtful under non-standard operating conditions, then the following algorithm can be used:

- Conduct experimental studies of the insulation material with temperature measurement on both sides of the insulation material;
- Create a mathematical model of the object and process. Verify the model with experimental data to determine material parameters such as thermal conductivity;
- Conduct numerical simulations to create dependencies of the minimum thickness of the insulating material depending on the desired temperature on the surface;
- If necessary, make additional clarifications to the model related to other methods of heat transfer (for example, convection and radiation), perform additional simulations and obtain new dependences of the parameters of the insulating material.

5. Conclusions

The carried out theoretical and experimental studies make it possible to calculate and analyze the required material thickness for thermal insulation of high-temperature networks and equipment. Based on the results of experimental studies, we built a model of heat transfer through the used insulating materials. Multiparametric calculations were carried out in a wide range of temperatures of the heated pipe and the thickness of the insulating material. The minimum insulation thickness was adjusted for the studied aerogel and basalt fiber materials. We have found that the passport data of the studied aerogel satisfactorily determine the minimum insulation thickness and the correction of the results is small. At the same time, the selected insulating material made of basalt fiber did not have passport data on the minimum thickness, and we used data from the methodology of SP 41-103-2000.

Aerogel surpasses basalt fiber in all key thermophysical and operational characteristics. Therefore, the only barrier to widespread industrial production and use of aerogel in the high-temperature thermal insulation segment is its market value, which, as a rule, is several times higher than the price of basalt fiber in terms of an equivalent volume of material. Taking these features into account when selecting thermal insulation operating at high temperatures (300–600 °C) will allow industrial enterprises to choose thermal insulation materials with optimal thermal, operational and economic characteristics.

The presented methodology and algorithm for determining the minimum thickness of the insulating material depending on the desired surface temperature can be useful

in practice when the data on the recommended insulation thickness are unknown or the passport data are doubtful under unstable operating conditions.

Our further research will be devoted to the development of the same methodology for asymmetric fully 3D geometric models of pipelines operating at high temperatures, as well as in non-stationary modes.

Author Contributions: Conceptualization, A.V.F., K.V.S., I.G.A. and U.B.; methodology, A.V.F., I.G.A. and U.B.; software, O.V.S., S.A.S. and M.D.Z.; validation, O.V.S. and S.A.S.; resources, M.D.Z. and D.V.G.; data curation, M.D.Z.; writing—original draft preparation, A.V.F. and K.V.S.; writing—review and editing, A.V.F., O.V.S. and S.A.S.; visualization, S.A.S. and A.V.F.; supervision, U.B.; funding acquisition, I.G.A. All authors have read and agreed to the published version of the manuscript.

Funding: This research was funded by the Ministry of Science and Higher Education of the Russian Federation within the framework of the state assignment No. 075-01262-22-01 from 28 January 2022 (Additional agreement 075-03-2022-151/1 from 31 January 2022).

Data Availability Statement: Not applicable.

Conflicts of Interest: The authors declare no conflict of interest.

References

1. Alattar, A.M. Spectral and structural investigation of silica aerogels properties synthesized through several techniques. *J. Non-Cryst. Solids* **2021**, *571*, 121048. [CrossRef]
2. Balaji, D.; Sivalingam, S.; Bhuvaneswari, V.; Amarnath, V.; Adithya, J.; Balavignesh, V.; Ganeshsurya, R. Aerogels as alternatives for thermal insulation in buildings—A comparative teeny review. *Mater. Today Proc.* **2022**, *62*, 5371–5377. [CrossRef]
3. Yang, W.; Liu, J.; Wang, Y.; Gao, S. Experimental study on the thermal conductivity of aerogel-enhanced insulating materials under various hygrothermal environments. *Energy Build.* **2020**, *206*, 109583. [CrossRef]
4. Groult, S.; Budtova, T. Thermal conductivity/structure correlations in thermal super-insulating pectin aerogels. *Carbohydr. Polym.* **2018**, *196*, 73–81. [CrossRef] [PubMed]
5. Cai, H.; Jiang, Y.; Feng, J.; Zhang, S.; Peng, F.; Xiao, Y.; Feng, J. Preparation of silica aerogels with high temperature resistance and low thermal conductivity by monodispersed silica sol. *Mater. Des.* **2020**, *191*, 108640. [CrossRef]
6. Wang, Y.; Wu, K.; Xiao, M.; Riffat, S.B.; Su, Y.; Jiang, F. Thermal conductivity, structure and mechanical properties of konjac glucomannan/starch based aerogel strengthened by wheat straw. *Carbohydr. Polym.* **2018**, *197*, 284–291. [CrossRef]
7. Fan, W.; Zhang, X.; Zhang, Y.; Zhang, Y.; Liu, T. Lightweight, strong, and super-thermal insulating polyimide composite aerogels under high temperature. *Compos. Sci. Technol.* **2019**, *173*, 47–52. [CrossRef]
8. Nguyen, S.T.; Do, N.D.; Thai, N.N.T.; Thai, Q.B.; Huynh, H.K.P.; Phan, A.N. Green aerogels from rice straw for thermal, acoustic insulation and oil spill cleaning applications. *Mater. Chem. Phys.* **2020**, *253*, 123363. [CrossRef]
9. Gupta, P.; Singh, B.; Agrawal, A.K.; Maji, P.K. Low density and high strength nanofibrillated cellulose aerogel for thermal insulation application. *Mater. Des.* **2018**, *158*, 224–236. [CrossRef]
10. Yoon, S.; Han, G.D.; Jang, D.Y.; Kim, J.W.; Kim, D.H.; Shim, J.H. Fabrication of yttria-stabilized zirconia aerogel for high-performance thermal barrier coating. *J. Alloys Compd.* **2019**, *806*, 1430–1434. [CrossRef]
11. Li, P.; Wu, H.; Liu, Y.; Yang, J.; Fang, Z.; Lin, B. Preparation and optimization of ultra-light and thermal insulative aerogel foam concrete. *Constr. Build. Mater.* **2019**, *205*, 529–542. [CrossRef]
12. Iswar, S.; Griffa, M.; Kaufmann, R.; Beltran, M.; Huber, L.; Brunner, S.; Malfait, W.J. Effect of aging on thermal conductivity of fiber-reinforced aerogel composites: An X-ray tomography study. *Microporous Mesoporous Mater.* **2019**, *278*, 289–296. [CrossRef]
13. Wei, G.; Liu, Y.; Zhang, X.; Yu, F.; Du, X. Thermal conductivities study on silica aerogel and its composite insulation materials. *Int. J. Heat Mass Transf.* **2011**, *54*, 2355–2366. [CrossRef]
14. Lakatos, Á.; Csík, A.; Csarnovics, I. Experimental verification of thermal properties of the aerogel blanket. *Case Stud. Therm. Eng.* **2021**, *25*, 100966. [CrossRef]
15. Berardi, U. The impact of aging and environmental conditions on the effective thermal conductivity of several foam materials. *Energy* **2019**, *182*, 777–794. [CrossRef]
16. Lakatos, Á. Stability investigations of the thermal insulating performance of aerogel blanket. *Energy Build.* **2019**, *185*, 103–111. [CrossRef]
17. Tugnoli, A.; Moricone, R.; Scarponi, G.E.; Cozzani, V. Effective thermal conductivity of fibrous fireproofing materials. *Int. J. Therm. Sci.* **2019**, *136*, 107–120. [CrossRef]
18. Yang, J.; Wu, H.; Xu, X.; Huang, G.; Xu, T.; Guo, S.; Liang, Y. Numerical and experimental study on the thermal performance of aerogel insulating panels for building energy efficiency. *Renew. Energy* **2019**, *138*, 445–457. [CrossRef]
19. Fesmire, J.E. Layered composite thermal insulation system for nonvacuum cryogenic applications. *Cryogenics* **2016**, *74*, 154–165. [CrossRef]

20. Wei, G.; Wang, L.; Xu, C.; Du, X.; Yang, Y. Thermal conductivity investigations of granular and powdered silica aerogels at different temperatures and pressures. *Energy Build.* **2016**, *118*, 226–231. [CrossRef]
21. Liao, H.; Chen, W.; Liu, Y.; Wang, Q. A phase change material encapsulated in a mechanically strong graphene aerogel with high thermal conductivity and excellent shape stability. *Compos. Sci. Technol.* **2020**, *189*, 108010. [CrossRef]
22. Kazemi, A.; Naseri, I.; Nasiri, M.; Bahramian, A.R. Effect of MgCl2 6H2O phase change material on thermal insulation performance of carbon aerogels. *J. Energy Storage* **2017**, *9*, 59–68. [CrossRef]
23. Liu, H.; Hu, M.; Jiao, J.; Li, Z. Geometric optimization of aerogel composites for high temperature thermal insulation applications. *J. Non-Cryst. Solids* **2020**, *547*, 120306. [CrossRef]
24. Zhang, Y.; Li, Y.; Lei, Q.; Fang, X.; Xie, H.; Yu, W. Tightly-packed fluorinated graphene aerogel/polydimethylsiloxane composite with excellent thermal management properties. *Compos. Sci. Technol.* **2022**, *220*, 109302. [CrossRef]
25. Hu, P.; Sun, Y.; Gao, B.; Gong, M.; Luo, B.; Fan, J. Novel monolithic yttria-alumina aerogel with low thermal conductivity made from inorganic precursors. *Ceram. Int.* **2022**, *48*, 18699–18703. [CrossRef]
26. He, H.; Geng, L.; Liu, F.; Ma, B.; Huang, W.; Qu, L.; Xu, B. Facile preparation of a phenolic aerogel with excellent flexibility for thermal insulation. *Eur. Polym. J.* **2022**, *163*, 110905. [CrossRef]
27. Yu, Y. *The Research and Development of Heat Insulation Materials with Low Thermal Conductivity in High Temperature*; Atlantis Press: Paris, France, 2015; Available online: https://www.atlantis-press.com/proceedings/mebe-15/sessions/345 (accessed on 11 September 2022).
28. Sharma, R.; Arch, B.; Berardi, U. The Use of Aerogel-Enhanced Blankets for Thermal Bridging Correction in Concrete & Steel Buildings. *Feature* **2019**, *21*, 59. Available online: https://www.semanticscholar.org/paper/The-Use-of-Aerogel-Enhanced-Blanket-for-Thermal-in-Sharma (accessed on 11 September 2022).
29. Zhang, L.; Zhu, L.; Zhang, C.; Wang, Z.; Xiao, P.; Liu, Z. Physical Experiment and Numerical Simulation on Thermal Effect of Aerogel Material for Steel Ladle Insulation Layer. *Coatings* **2021**, *11*, 1205. [CrossRef]
30. Berardi, U.; Nosrati, R.H. Long-term thermal conductivity of aerogel-enhanced insulating materials under different laboratory aging conditions. *Energy* **2018**, *147*, 1188–1202. [CrossRef]
31. Lakatos, Á.; Csarnovics, I. Infuence of thermal annealing on structural properties of silica aerogel super insulation material. *J. Therm. Anal. Calorim.* **2020**, *142*, 321–329. [CrossRef]
32. Pyo, Y.; Robertson, T.; Yun, S.; Hong, Z. Experimental Evaluation of Using Silica Aerogels as the Thermal Insulator for Combustor Liners. *J. Glob. Power Propuls. Soc.* **2020**, *4*, 202–216. [CrossRef]
33. Wiener, M.; Reichenauer, G.; Braxmeier, S.; Hemberger, F.; Ebert, H.-P. Carbon Aerogel-Based High-Temperature Thermal Insulation. *Int. J. Thermophys.* **2009**, *30*, 1372–1385. [CrossRef]
34. Vankov, Y.; Bazukova, E.; Emelyanov, D.; Fedyukhin, A.; Afanaseva, O.; Akhmetova, I.; Berardi, U. Experimental Assessment of the Thermal Conductivity of Basalt Fibres at High Temperatures. *Energies* **2022**, *15*, 2784. [CrossRef]
35. Yanhu, M.; Guoyu, L.; Wei, M.; Zhengmin, S.; Zhiwei, Z.; Wang, F. Rapid permafrost thaw induced by heat loss from a buried warm-oil pipeline and a new mitigation measure combining seasonal air-cooled embankment and pipe insulation. *Energy* **2020**, *203*, 117919. [CrossRef]
36. Yarahmadi, N.; Vega, A.; Jakubowicz, I. Determination of essential parameters influencing service life time of polyurethane insulation in district heating pipes. *Energy Procedia* **2017**, *116*, 320–323. [CrossRef]
37. Farouk, M.; Soltan, A.M.; Schlüter, S.; Hamzawy, E.; Farrag, A.; El-Kammar, A.; Yahya, A.; Pollmann, H. Optimization of microstructure of basalt-based fibers intended for improved thermal and acoustic insulations. *J. Build. Eng.* **2021**, *34*, 101904. [CrossRef]
38. Xing, D.; Chang, C.; Xi, X.-Y.; Hao, B.; Zheng, Q.; Gutnikov, S.I.; Lazoryak, B.I.; Ma, P.-C. Morphologies and mechanical properties of basalt fibre processed at elevated temperature. *J. Non-Cryst. Solids* **2022**, *582*, 121439. [CrossRef]
39. Wang, W.; Wang, Y.; Chen, Q.; Liu, Y.; Zhang, Y.; Ma, G.; Duan, P. Bond properties of basalt fiber reinforced polymer (BFRP) bars in recycled aggregate thermal insulation concrete under freeze–thaw cycles. *Constr. Build. Mater.* **2022**, *329*, 127197. [CrossRef]
40. Guan, H.; Xiao, T.; Luo, W.; Gu, I.; He, R.; Xu, P. Automatic fault diagnosis algorithm for hot water pipes based on infrared thermal images. *Build. Environ.* **2022**, *218*, 109111. [CrossRef]
41. Yu, X.; Tian, X. A fault detection algorithm for pipeline insulation layer based on immune neural network. *Int. J. Press. Vessel. Pip.* **2022**, *196*, 104611. [CrossRef]
42. Yu, X.; Lu, Y.H.; Gao, Q. Pipeline image diagnosis algorithm based on neural immune ensemble learning. *Int. J. Press. Vessel. Pip.* **2021**, *189*, 104249. [CrossRef]
43. Yu, X.; Ye, X.; Gao, Q. Pipeline image segmentation algorithm and heat loss calculation based on gene-regulated apoptosis mechanism. *Int. J. Press. Vessel. Pip.* **2019**, *172*, 329–336. [CrossRef]